# On the nature of ionic liquid gating of Nd2−xCexCuO4 thin films

Atesci, H.; Coneri, F.; Leeuwenhoek, M.; Hilgenkamp, H.; Ruitenbeek, J.M. van

# On the nature of ionic liquid gating of $Nd_{2-x}Ce_xCuO_4$ thin films

Hasan Atesci,[†] Francesco Coneri,[‡] Maarten Leeuwenhoek,[†] Hans Hilgenkamp,[‡] and Jan M. van Ruitenbeek[*,†]

E-mail: ruitenbeek@physics.leidenuniv.nl

**Abstract**

Recently, ionic liquid gating has been used to modulate the charge carrier properties of metal oxides. The mechanism behind it, however, is still a matter of debate. In this paper, we report experiments on doped and undoped $Nd_2CuO_4$. We find major resistance drops of the bilayer coupled to observations of the presence of a considerable Faradeic component in the gate current and of the appearance of charge transfer peaks in the cyclic voltammetry data. This lead us to propose a mechanism of gating based on irreversible electrochemical reactions, likely due to trace amounts of contaminations present in the ionic liquid. This work is therefore in line with previous reports confirming the presence of irreversible electrochemistry in ionic liquid gated electron-doped cuprates.

Since its discovery in 1986,[1] high temperature superconductivity (HTS) in doped Mott-insulator cuprates has generated much interest.[2] Although the mechanism of pairing remains illusive,[3–6] many of its characteristics have been firmly established. Cuprate HTS can be either hole-doped or electron-doped, and typically shows a dome-shaped phase diagram as a function of chemical

[*]To whom correspondence should be addressed

[†]Huygens-Kamerlingh Onnes Laboratorium, Universiteit Leiden, Postbus 9504, 2300 RA Leiden, The Netherlands

[‡]MESA+ Institute for Nanotechnology, University of Twente, University of Twente, P.O. Box 217, 7500 AE Enschede, The Netherlands

doping.[7] However, chemical doping induces disorder in the Mott-insulator compound,[8] which can be avoided by electrostatically doping the HTS using an oxide gate dielectric[9–12]. Oxide gate dielectrics have successfully achieved changes in the critical temperature of cuprates.[13] But, due to the break down electric field,[14,15] the induced charge carrier density is limited to $\sim$10$^{13}$ cm$^{-2}$, having only a relatively small influence on the changes on the conductive properties of the cuprate.[16] This is due to the fact that the charge carrier density in Mott insulator cuprates requires an areal density of up to 10$^{14}$ cm$^{-2}$ in order to go through the phase diagram of HTS cuprates. To overcome this problem, ionic liquids (ILs) have recently been used as gate media to generate high carrier accumulation.[17,18] ILs consist entirely of ions, and when a voltage is applied across the IL, Helmholtz electric double layers are formed (Fig.2A). These layers consist of ions of one kind of the IL and the induced charge carriers of the solid and are separated $\sim$1 nm from each other. With IL gating, carrier densities of up to $8\times10^{14}$ cm$^{-2}$ are achievable,[17] substantially higher than what is attainable with their conventional dielectric counterparts, making it possible to induce insulator-to-superconductor transitions.[19–21]

In this work, we attempt to address two points of interest. Firstly, most of the IL experiments on cuprates have been done on hole-doped cuprates,[19,22,23] whereas for electron-doped compounds only $Pr_{2-x}Ce_xCuO_4$ and $NdBa_2Cu_3O_{7-\delta}$ have been tested with ILs.[24–26] Hence, IL gating on electron-doped cuprate compounds is important for obtaining a more complete picture of its effects on cuprates and high-temperature superconductors in general. Secondly, there is an increasing number of articles stating that the effect of IL gating in cuprates and other oxides is related to electrochemistry,[26–31] indicating that the ideal picture of EDL electrostatics suggested in some articles[19–21,23] might not be valid.

We have applied the IL gating technique at the pulsed laser deposition (PLD) grown electron-doped cuprate of single layers of undoped $Nd_2CuO_4$ (NCO) and bilayers of 0.10 Ce doped $Nd_{2-x}Ce_xCuO_4$ ($x = 0.10$) (NCCO) and NCO (NCCO/NCO). We have used a deposition temperature of 820 °C and $O_2$ pressure of 2.5 $\times10^{-1}$ mbar. The NCO and NCCO targets are ablated using a laser fluence of $\sim$ 1.2 J/cm$^{-2}$ and repetition rate of 4 Hz. The cuprate is grown on substrates formed by a pristine $(LaAlO_3)_{0.3}(Sr_2TaAlO_6)_{0.7}$ (001) (LSAT) crystal. The cuprate and substrate have lattice parameters

of 3.94 Å and 3.87 Å, leading to some epitaxial strain in NC(C)O. For the reason of lowering the epitaxial strain of the upper layers, we have grown the bilayers.[23,32–34]

By varying the lens and mask positions and the energy of the laser beam, we can influence the spot size of the laser beam, while keeping the laser fluence constant at 1.2 mJ/cm$^{-2}$. We observe that a lower spot size and a lower energy leads to a lower growth rate of the compound per pulse, and is in general more suitable for layer-by-layer growth. For our system, we find a growth rate of 0.5 Å per pulse using optimized settings (spot size of 2.2 mm$^2$ and an energy of 29.3 mJ) for layer-by-layer growth. To monitor the in-situ growth of the cuprate, we have used Refractive High Energy Electron Diffraction (RHEED) Fig. 1A. The intensity of the specular reflected beam shows clear oscillations for the first unit cells of the compound. The amplitude of these oscillations quickly dies out, indicating a transition from layer-by-layer growth to island-like growth fashion. For the thicknesses of the films we are interested in, the resulting morphology of the films is characterized by screw dislocations, showing the spiral growth mode of the cuprate grains Fig. 1B, and is similar to what is found for cuprates grown on substrates having lattice mismatches.[35,36]

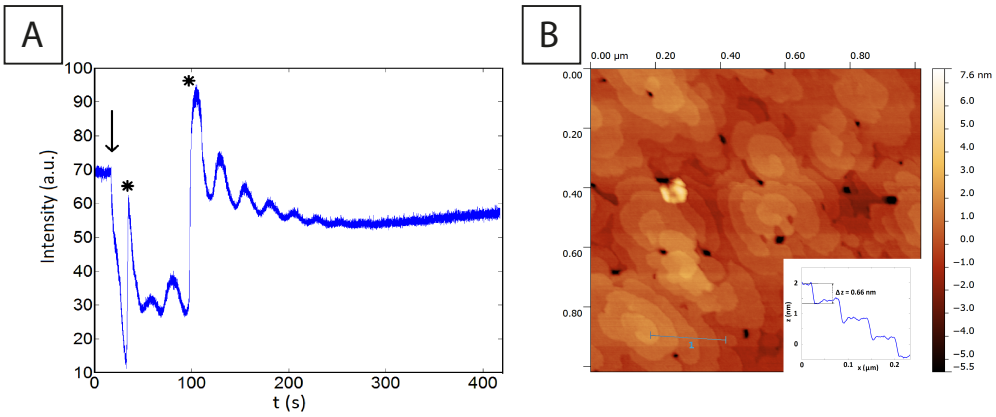


Figure 1: A) RHEED intensity vs. time graph which shows the oscillations of the specular reflected beam for the first few unit cells of the cuprate, after which the amplitude of the oscillation goes to zero, indicating an island-like growth fashion. The arrow indicates the start of the PLD process, while the asterisks show the instances where the electron beam intensity has been increased manually. B) The AFM data shows the screw-island growth mode of a typical cuprate film on LSAT. The step heights coincide with half a unit cell of NC(C)O (1.2 nm).

We have tested a total of 22 samples, where the NCO single layers have thicknesses varying from 12 to 48 unit cells, while NCCO/NCO bilayers have bottom layers that are 24 to 46 unit cells

thick and top layers that are 4 to 12 unit cells thick. We show that IL gating has an effect in lowering the resistance of a bilayer of the compound, and we argue that this is caused by electrochemical reactions, likely because of trace amounts of impurities present in the IL. The results shown in this paper are for a particular NCCO/NCO bilayer of 20 unit cells thick NCO and 5 unit cells thick NCCO, and is reproducible for the other samples, unless stated otherwise.

After PLD deposition, we use photolithography to define areas on the sample that will be maintained, while the rest is removed by argon ion milling. In order to decrease the contact resistance, all of the remaining bilayer is covered by sputter deposition of Ti/Au, apart from the bilayer of the channel area. In order to prevent unnecessary leakage currents, the substrate surface is then covered by an insulating photoresist layer, except for the gate electrode and channel (Fig. 2A). The exposed areas are chemically etched in an oxygen plasma (100 mTorr, 13 W) which removes any residuals of the photolithographic process.

The sample is then placed inside a $N_2$ atmosphere glovebox (<0.1 ppm $O_2$ , $H_2O$),where it is heated to 120 $^\circ$ C to remove any water on top of the surface. The ionic liquid bottle containing N,N-diethyl-N-(2-methoxyethyl)-N-methylammoniumbis(trifluoromethyl- sulphonyl)imide (DEME-TFSI), is kept in the same atmosphere. Before any usage of the IL, it is preheated at 60 $^\circ$C for a period of more than 72 hours. With the insertion of a needle in the IL bottle, a small droplet is formed at the end of the needle, which is then put on top of the gate electrode and the bilayer channel area (Fig. 2B). Next, the sample is transported to the insert chamber of the measurement setup, which is flushed with He gas and pumped several times to remove contaminations ($O_2$ and $H_2O$) from the atmosphere of the sample.

We use two Keithley 2400 SourceMeters for the experiments. One SourceMeter is used to measure the four terminal resistance of the channel. To this end, we apply a current bias between the source and drain electrodes (500 nA), while limiting the maximum voltage $V_{sd}$ to 250 mV. We use the other SourceMeter for the application of a gate voltage $V_g$ and monitoring the gate current $I_g$. In order to limit electrochemical processes influencing carrier doping of the channel, the maximum $V_g$ applied is 2.5 V, which lies well within the potential window of the liquid.[37,38] Furthermore, the

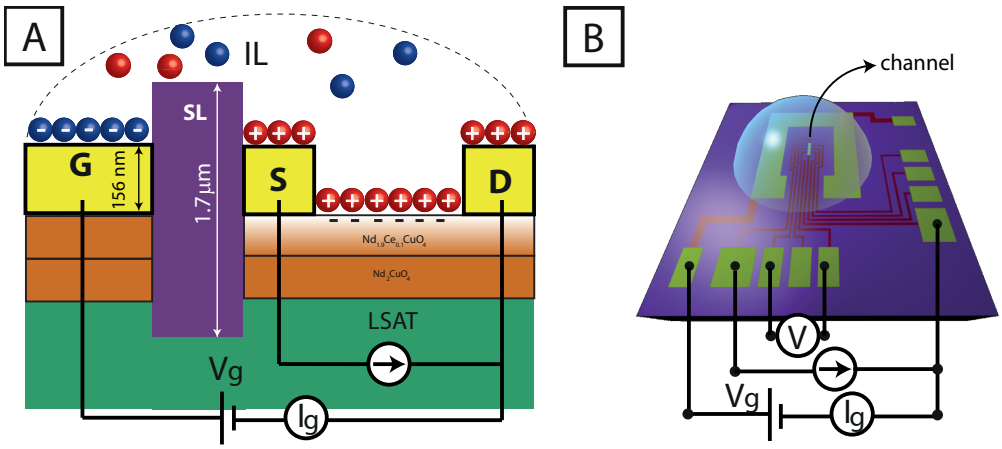


Figure 2: A) A schematic cross section of the sample. Here, yellow and blue spheres represent TFSI(-) and DEME(+) ions, respectively. The gate (G), source (S) and drain (D) electrodes are 6 nm (Ti) + 150 (Au) nm thick and are made using photolithograpy after deposition of the bilayer. A separator layer (SL) ensures only the bilayer channel at the surface of the NCCO between the source and drain electrodes is in contact with the ionic liquid droplet. Applying a voltage between the gate and drain electrodes leads to a charge buildup in the channel. B) A schematic top view of the sample. Except for the large Au gate electrode around the center of the sample, the Au contacts at the sides of the samples, and the channel area near the center, the whole surface is covered by a hard-baked photoresist layer. The contacts at the sides are connected to a Hall bar configuration of electrodes on the channel to measure electronic properties of the channel area of the bilayer, which is freed from photolithographic residuals by oxygen plasma etching. A current is sent through the source (S) and drain (D) electrodes. In combination with voltage probes placed at one side of the sample, the four-point resistance of the channel is measured, having an area of 50 x 300 $\mu m^2$. The gate electrode, has an exposed area of more than 100 times the area of the exposed NCCO channel.

experiments are performed at a suitable charging temperature of 210 K,[39] above the melting point of DEME-TFSI of 184 K.[40]

Our measurement comprises five cycles of two sub measurements. The first sub measurement is in-situ cyclic voltammetry (CV) in order to test for possible chemical reactions in the Au/IL/bilayer system.[41] During the CV, $I_g$ is measured while modulating $V_g$ from 0 V to 2.5 V and back to 0 V again at a scan rate of 5 mV/s. The second sub measurement records the $I_g(t)$ and four terminal resistance $R(t)$ characteristics of the channel after switching the gate voltage from zero to +0.5 V, +1.0 V, +1.5 V, +2.0 V and +2.5 V for 15 minutes. After the second sub measurement is finished, the Keithley instruments are reset to zero for approximately 30 minutes. The relaxation time of the charges in the IL can be estimated by $R_{IL}C_{EDL}$, where $R_{IL}$ is the resistance of the IL, approximated to be in the order of $10^9$ $\Omega$.[42] The electric double layer capacitance is estimated as 2 nF, since the channel area is 1.5 $\times 10^{-4}$ cm$^{-2}$ and the specific capacitance is 13 $\mu F$ cm$^{-2}$. Thus, the RC time is in the order of seconds, making the waiting time of 30 minutes sufficiently long to cancel any memory effect of the ions.

The CV data in Fig. 3 indicates the presence of irreversible reactions. This is based on the fact the the first cyclic voltammogram does not show any peaks, indicating that the IL is clean and that no electrochemical reactions take place in the initial stages of the experiment. The subsequent CVs do show peaks, denoted as peaks I (cathodic), II and III (both anodic). Peak I is located between 1.35 and 1.95 V and indicates an initial reduction. Peak II and III are located between 1.1 and 1.435 V, and 0.29 and 0.55 V, respectively. If peak I would be caused by a reversible reaction, only one anodic peak would be expected. However, we see two anodic peaks, indicating the oxidation of either the product(s) or a part of the product(s) of this reduction. Furthermore, if peaks I and II are part of the same reversible reaction, the Nernst equation would dictate that for reversible electrochemistry the difference in potential of the anodic and cathodic peaks lies within $0.059$ V.[43] Moreover, one would expect that both peaks are equal in amplitude. The CV data shows however, that the potential separation of both peaks (I and II) is $0.27<\Delta V<0.51$ V, while the magnitude of peak I is approximately 3 to 10 times larger than peak II for all CV scans.

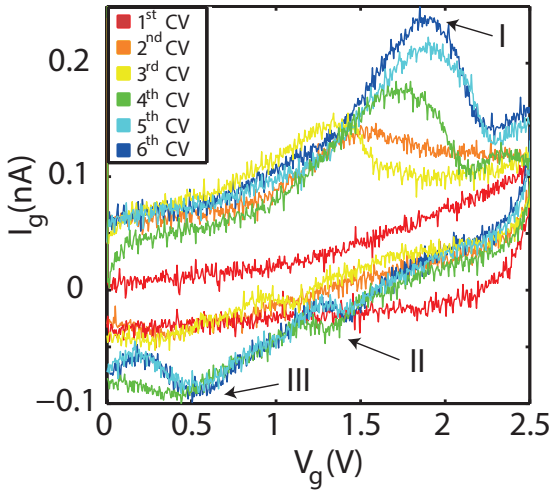


Figure 3: Plots showing 6 CV scans. The first cyclic voltammogram does not show any peaks and indicates a chemically pure IL, while the others show peaks increasing in amplitude as a function of the cycle number. As the number of CV scans increases, several peaks (I, II and III) start to appear. Peak I is located between 1.35 and 1.95 V and indicates an initial reduction. Peak II and III are located between 1.1 and 1.435 V, and 0.29 and 0.55 V, respectively. We observe that the potential separation between peaks I and II is $0.27<\Delta V<0.51$ V. Furthermore, the amplitude of peak I is a factor 3 to 10 higher than that of peaks II and III.

The presence of irreversible electrochemistry is further supported by AFM data. (Fig. 4A) shows an image of the surface of a freshly prepared sample, with structure typical for island growth of the films. The importance of this observation is that the edges of the islands expose sites with higher reactivity, which could act as possible seeding locations for electrochemical reactions. Before the experiment, the sample surface topography showed a root mean squared (rms) roughness value of 0.87 nm (Fig. 4A). After the IL gating experiments, the surface is altered dramatically, having a substantially higher rms roughness value of 2.35 nm (Fig. 4B).

Another argument for electrochemistry is based on our gate current vs. time data. After switching the gate voltage to the set value at the start of the second sub measurement, the gate current data shows a rapid initial decrease, followed by a slowly decaying function, a typical graph of which is shown in Fig. 5. In case the charging process is strictly electrostatic, the total accumulated charge would be given by $Q = ACV_g$. Here, $A$ is the total NCCO area and $C$ is the specific capacitance, being equal to 1.5 $\times 10^{-4}$ cm$^2$ and 13 $\mu F$ cm$^{-2}$,[44] respectively, making the expected charge

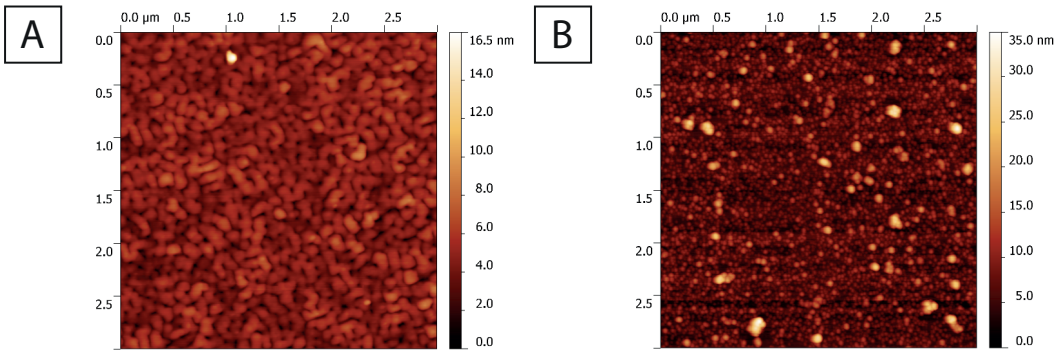


Figure 4: AFM images of the surface of the bilayer before (A) and after (B) IL gating experiments. A) Before the experiments, the AFM image shows that NCCO has a topography which is island-based. The roughness of the sample is 0.87 nm. B) After the experiments, the surface lost the former characteristics, and has a higher roughness of 2.35 nm.

roughly 5 nC for the highest gate voltages used. The observed charge, calculated as the integral of $I_g$, however, is typically one to two orders of magnitude higher for all measurements, suggesting other mechanisms, notably electrochemical reactions, play a role.

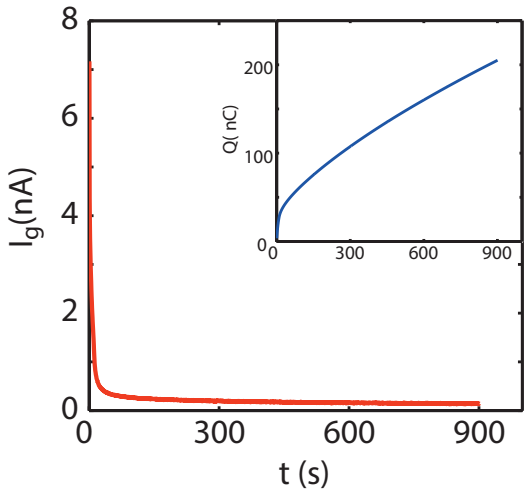


Figure 5: A) $I_g(t)$ curve for a $V_g$ of 2.5 V at 210 K. The inset shows the total accumulated charge $Q$ vs. time, calculated by integrating $I_g(t)$. The total accumulated charge $Q$ exceeds the value that one would expect for a purely electrostatic charge of the NCCO layer, i.e. roughly 5 nC.

We find that the $I_g(t)$ characteristic cannot be fitted with only an exponential term, indicative of electrostatic charging of the bilayer. Rather, we need to add a Faradeic, diffusive, term with a certain proportionality constant $K$, i.e. $I(t) = K/\sqrt{t}$ to fit the whole curve, with

$$K = \frac{cAF\sqrt{D}}{\sqrt{\pi}}$$

.

Here, $c$ is the concentration of the substance taking part in the electrochemical reaction $A$ is the area of the bilayer surface, $F$ is the Faraday constant, and $D$ is the diffusion coefficient of the reactive species. We find that the proportionality constant for all of the curves is between 0.04 < K < 1.4 nA $s^{\frac{1}{2}}$. The large spread in this parameter is due to the fact that it is gate voltage dependent, where a larger applied gate voltage would lead to higher gate currents and therefore higher proportionality constants. If we assume the cations and anions of the IL are taking part in the reaction, we come to the conclusion that the desired diffusion constant of the species should be $10^{-\beta}$ $cm^2/s$, with $\beta$ = 14-18. In this calculation, we take an approximate value for the density of the IL to be 1.5 $g/cm^{-3}$. The obtained value of $D$, however, is many orders of magnitude below the expected literature values for DEME-TFSI, which is $10^{-\beta}$ $cm^2/s$, with $\beta$ = 8.6 - 10.6.[45,46] Because of this difference in diffusion coefficient values, it is not plausible that the anions and cations of the IL take part in the irreversible reaction. A more likely scenario is that trace amount of impurities like hydrogen and oxygen present in the IL react with the surface. Indeed, it has been shown that impurities of hydrogen can lead to major gating effects in oxides,[28,47,48] while oxygen impurities can lead to either the doping of oxygen,[49] or the generation of oxygen vacancies.[29,31,50] Although it has been shown that both hydrogenation[51] and (de)oxygenation[52] are applicable to NCCO, it is not possible to deduce which of these processes are present in the present system with our current techniques.

In Fig. 6A we show that the resistance $R$ systematically decreases an amount $\Delta R$ when a positive gate voltage is applied. Here, $\Delta R$ is the difference between $R$ at $t = 0$ s ($R_0$) and the value of the tangent line at $t = 0$ s of $R$ at $t = 900$ s. In the next figure, the relative change of $R$ is plotted as a function of cycle number and $V_g$ (Fig. 6B). The conductance gains in the first cycle are limited and the relative change in $R$ is 5 % at the highest $V_g$ of +2.5 V. However, as the cycle number is increased, the relative change in $R$ shows a systematic increase as a function of both $V_g$ and the

cycle number, having a relative change close to 25 % at +2.5 V. This clearly shows the irreversibility of the gating effect, while reversibility is expected in case the gating would be electrostatic. This behavior is typical for single-layered channels of NCO as well. We also observe that the relative change of $R$ is larger for samples that have been tested with a lower degree of purification of IL, again indicating that impurities play a major role in the effect. In Fig. 6C we plot the normalized resistance vs. temperature of the gated bilayer. In this figure, we observe semiconducting behavior down to 10 K. For gate voltages up to +2.0 V we observe a systematic decrease of the resistance, but no onset of superconductivity, while a film similar in doping without being gated did become superconductive below 12 K (inset of Fig. 6C). The application of a higher gate voltage ($V_g \cong 2.5$ V) leads to sample degradation.

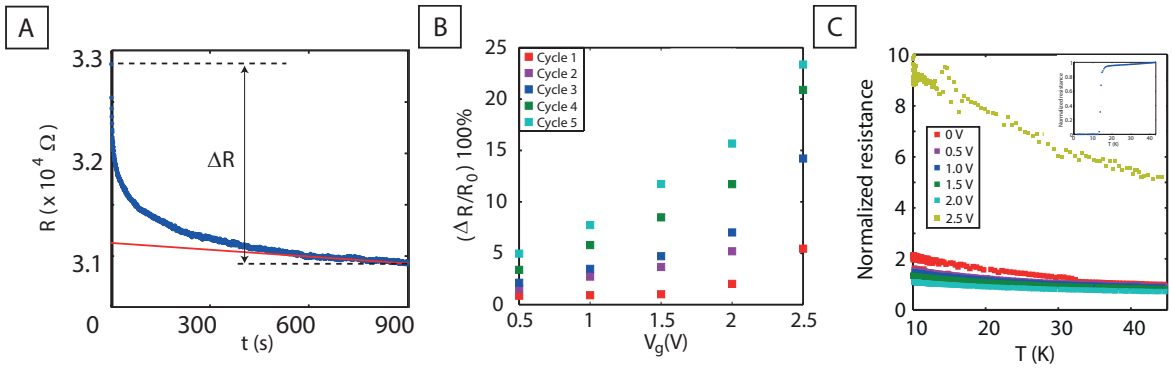


Figure 6: A) $R(t)$ curve recorded when at $t = 0$ s a $V_g$ of 0.5 V is applied. The curve shows a change $\Delta R$, defined as the difference between $R$ at $t = 0$ s ($R_0$) and the value of the tangent line at $t = 0$ s of $R$ at $t = 900$ s. B) The observed relative change in $R$ as a function of gate voltage and cycle number at 210 K. The change in $R$ is systematic and becomes larger as $V_g$ and the number of cycles increases. C) Normalized resistance of the NCCO/NCO channel plotted as a function of $T$ for $V_g$ = 0 V, +0.5 V, +1.0 V, +1.5 V, +2.0 V and +2.5 V. The behavior is semiconductor-like, and shows a systematic decrease of the resistance up to a gate voltage of +2.0 V. However, applying a gate voltage of +2.5 V leads to sample degradation. The inset figure shows the same type of graph for a film of similar doping which has not been IL gated, showing a critical temperature onset of 12 K.

In summary, we have applied IL gating on the single layers of NCO and bilayers NCCO/NCO. We observe that repeated gating leads to the appearance of peaks in the cyclic voltammogram. These reactions have a substantial influence in the resistance of the NCCO layer, especially after a prolonged period of gating, which goes hand in hand with pronounced distortions of the NCCO

surface. Together with these observations, we see that accumulated charge in the system that far exceeds the expected electrostatic accumulation. All of these point to the presence of irreversible electrochemical reactions. The fitting of the gate current data indicates that these are caused by traces of impurities in the ionic liquid. With the present technique of PLD growth of the material and the choice of substrate, we have found that it is not possible to obtain layer-by-layer growth, which would help prevent electrochemical reactions happening in the compound. This work confirms previous work done on electron-doped cuprates of $NdBa_2Cu_3O_{7-x}$ and $Pr_{2-x}Ce_xCuO_4$. In the former material, IL gating has been found to produce oxygen vacancies. In $Pr_{2-x}Ce_xCuO_4$, gate voltages above + 2.5 V lead to irreversible electrochemical reactions.[24] Similarly, using gate voltages below + 2.5 V leads to a relatively little gating effect, not enough to induce a superconducting transition.[25]

## Acknowledgement

This work is part of the research programme of the Foundation for Fundamental Research on Matter (FOM, 12PR3047), which is financially supported by the Netherlands Organization for Scientific Research (NWO). The authors also gratefully acknowledge the technical support from J. Aarts and S. Voltan.

## References

(1) Bednorz, J.; Müller, K. A. *Z. Phys. B: Condens. Matter* **1986**, *64*, 189.

(2) Dagotto, E. *Review of Modern Physics* **1994**, *66*, 763–840.

(3) Scalapino, D. J. *Phys. Rep.* **1995**, *250*, 329.

(4) Kastner, M. A.; Birgeneau, R. J.; Shirane, G.; Endoh, Y. *Rev. Mod. Phys.* **1998**, *70*, 897.

(5) Timusk, T.; Statt, B. *Rep. Prog. Phys.* **1999**, *62*, 61.

(6) Orenstein, J.; Millis, A. J. *Science* **2000**, *288*, 468.

(7) Ahn, C. H.; Bhattacharya, A.; Ventra, M. D.; Eckstein, J. N.; Frisbie, C. D.; Gershenson, M. E.; Goldman, A. M.; Inoue, I. H.; Mannhart, J.; Millis, A. J.; Morpurgo, A. F.; Natelson, D.; Triscone, J. M. *Review of Modern Physics* **2006**, *78*, 1185–1212.

(8) Ueno, K.; Nakamura, S.; Shimotani, H.; Yuan, H. T.; Kimura, N.; Nojima, T.; Aoki, H.; Iwasa, Y.; Kawasaki, M. *Nature Nanotechnology* **2011**, *6*, 408–412.

(9) Matthey, D.; Gariglio, S.; Triscone, J. *Applied Physics Letters* **2003**, *83*, 3758.

(10) Salluzzo, M.; Cassinese, A.; Luca, G. M. D.; Gambardella, A.; Prigiobbo, A.; Vaglio, R. *Physical Review B* **2004**, *70*, 214528.

(11) Cassinese, A.; Luca, G. M. D.; Prigiobbo, A.; Salluzzo, M.; Vaglio, R. *Applied Physics Letters* **2004**, *84*, 3933–3935.

(12) J.Mannhart,; J.G.Bednorz,; K.A.Miiller,; D.G.Schlom, *Z. Phys. B* **1991**, *83*, 307–311.

(13) Mannhart, J. *Supercond. Sci. Technol.* **1996**, *9*, 46–67.

(14) Lin, H. C.; Ye, P. D.; Wilk, G. D. *Applied Physics Letters* **2005**, *87*, 182904.

(15) Wu, Y. H.; Yang, M. Y.; Chin, A. *IEEE Electron Device Letters* **2000**, *21*, 341–343.

(16) V.C.Matijasevic,; S.Bogers,; N.Y.Chen,; H.M.Appelboom,; P.Hadley,; J.E.Mooij, *PhysicaC* **1994**, *235-240*, 2097–2098.

(17) Yuan, H.; Shimotani, H.; Tsukazaki, A.; Ohtomo, A.; Kawasaki, M.; Iwasa, Y. *Advanced Functional Materials* **2009**, *19*, 1046–1053.

(18) Shimotani, H.; Asanuma, H.; Tsukazaki, A.; Ohtomo, A.; Kawasaki, M.; Iwasa, Y. *Applied Physics Letters* **2007**, *91*, 082106.

(19) Leng, X.; Garcia-Barriocanal, J.; Bose, S.; Lee, Y.; Goldman, A. M. *Physical Review Letters* **2011**, *107*, 027001.

(20) Garcia-Barriocanal, J.; Kobrinskii, A.; Leng, X.; Kinney, J.; Yang, B.; Snyder, S.; Goldman, A. M. *Physical Review B* **2013**, *87*, 024509.

(21) Dubuis, G.; Bollinger, A. T.; Pavuna, D.; Misewich, J.; Bozovič, I. *Journal of Applied Physics* **2012**, *111*, 112632.

(22) Garcia-Barriocanal, J.; Kobrinskii, A.; Leng, X.; Kinney, J.; Yang, B.; Snyder, S.; Goldman, A. M. *Physical Review B* **2013**, *87*, 024509.

(23) Bollinger, A. T.; Dubuis, G.; Yoon, J.; Pavuna, D.; Misewich, J.; Bozovič, I. *Nature* **2011**, *472*, 458–460.

(24) Jin, K.; Hu, W.; Zhu, B.; Kim, D.; Yuan, J.; Sun, Y.; Xiang, T.; Fuhrer, M. S.; Takeuchi, I.; Greene, R. L. *Scientific Reports* **2016**, *6*, 26642.

(25) Zeng, S. W.; Huang, Z.; Lv, W. M.; Bao, N. N.; Gopinadhan, K.; Jian, L. K.; Herng, T. S.; Liu, Z. Q.; Zhao, Y. L.; Li, C. J.; Ma, H. J. H.; Yang, P.; Ding, J.; Venkatesan, T.; Ariando, *Physical Review B* **2015**, *92*, 020503.

(26) Zhang, L.; Zeng, S. W.; Wan, D. Y.; Han, K.; Jian, L. K.; Ariando, A.; Venkatesan, T. APS March Meeting 2016, http://meetings.aps.org/link/BAPS.2016.MAR.V25.11.

(27) Zhou, Y.; Ramanathan, S. *J. of Applied Physics* **2012**, *111*, 084508.

(28) Ji, H.; Wei, J.; Natelson, D. *Nano Letters* **2012**, *12*, 2988–2992.

(29) Jeong, J.; Aetukuri, N.; Graf, T.; Schladt, T. D.; Samant, M. G.; Parkin, S. S. P. *Science* **2013**, *339*, 1402–1405.

(30) Nakano, M.; Shibuya, K.; Okuyama, D.; Hatano, T.; Ono, S.; Kawasaki, M.; Iwasa, Y.; Tokura, Y. *Nature* **2012**, *487*, 459–462.

(31) Ueno, K.; Shimotani, H.; Iwasa, Y.; Kawasaki, M. *Applied Physics Letters* **2010**, *96*, 252107.

(32) Sato, H.; Yamamoto, H.; Naito, M. *Physica C* **1997**, *274*, 227.

(33) Rüfenacht, A.; Chappatte, P.; Gariglio, S.; Leemann,; Fompeyrine, J.; Locquet, J.-P.; Martinoli, *Solid-State Electron* **2003**, *47*, 2167.

(34) Jaccard, Y.; Cretton, A.; Williams, E. J.; Locquet, J.-P.; Mächler, E.; Gerber, C.; Schneider, T.; Fischer, O.; Martinoli, P. *Proc. SPIE* **1994**, *2158*, 200.

(35) Prijamboedi, B.; Kashiwaya, S. *J Mater Sci: Mater Electron* **2006**, *17*, 483–488.

(36) Luo, L.; Hawley, M. E.; Maggiore, C. J.; Dye, R. C.; Muenchausen, R. E.; Chen, L.; Schmidt, B.; Kaloyeros, A. E. *Appl. Phys. Lett.* **1993**, *62*, 1993.

(37) Polat, E. O.; Balcı, O.; Kocabas, O. *Sci. Rep.* **2014**, *4*, DOI: 10.1038/srep06484.

(38) Ye, J. T.; Inoue, S.; Kobayashi, K.; Kasahara, Y.; Yuan, H. T.; Shimotani, H.; Iwasa, Y. *Nature Materials* **2010**, *9*, 125–128.

(39) Dubuis, G.; Bollinger, A. T.; Pavuna, D.; Bozovič, I. *J. of Applied Physics* **2012**, *111*, 112632.

(40) Sato, T.; Masuda, G.; Takagi, K. *Electrochimica Acta* **2004**, *49*, 3603–3611.

(41) Rusling, J. F.; Suib, S. L. *Adv. Mat.* **1994**, *6*, 922–930.

(42) Yuan, H.; Shimotani, H.; Ye, J.; Yoon, S.; Aliah, H.; Tsukazaki, A.; Kawasaki, M.; Iwasa, Y. *J. Am. Chem. Soc.* **2010**, *132*, 18402–18407.

(43) Kissinger, P. T.; Heineman, W. R. *J. Chem. Education* **1983**, *60*, 702–706.

(44) Tsuchiya, T.; Ochi, M.; Higuchi, T.; Terabe, K.; Aono, M. *ACS Appl. Mater. Interfaces* **2015**, *7*, 12254–12260.

(45) Hayamizu, K.; Tsukuzi, S.; Seki, S.; Ohno, Y.; Miyashiro, H.; Kobayashi, Y. *J. Phys. Chem. B* **2008**, *112*, 1189–1197.

(46) Hayamizu, K.; Tsukuzi, S.; Seki, S. *J. Chem. Eng. Data* **2014**, *59*, 1944–1954.

(47) Meng, X.; Quenneville, F.; Venne, F.; Mauro, E. D.; Işık, D.; Barbosa, M.; Drolet, Y.; Natile, M. M.; Rochefort, D.; Soavi, F.; Santo, C. *J. Phys. Chem. C* **2015**, *119*, 21732–21738.

(48) Katase, T.; Endo, K.; Tohei, T.; Ikuhara, Y.; Ohta, H. *Adv. Electron. Mater.* **2015**, *1*, 1500063.

(49) Shi, J.; Ha, S. D.; Zhou, Y.; Schoofs, F.; Ramanathan, S. *Nature Communications* **2013**, *472*, 458–460.

(50) Li, M.; Han, W.; Jeong, J.; Samant, M. G.; Parkin, S. S. P. *Nano Letters* **2013**, *13*, 4675–4678.

(51) Kobayashi, K.; Goto, Y.; Matsushima, S.; Okada, G. *J. Mat. Sci. Letters* **1991**, *10*, 523–525.

(52) Jian, W.; Mao, S. N.; Xi, X. X.; Jian, X.; Peng, J. L.; Venkatesan, T.; Lobb, C. J.; Greene, R. L. *Physical Review Letters* **1994**, *4*.